Materials Advances

ROYAL SOCIETY OF CHEMISTRY

PAPER

View Article Online
View Journal

Cite this: DOI: 10.1039/d6ma00205f

Design and fabrication of a polyaniline-grafted nanocarbon material for energy harvesting applications

Tien Hung Nguyen, †[ae] Thanh Huy Nguyen, †[ae] Bui Anh Duy Nguyen, [ae] Thi Cam Linh Tran,[ae] Thanh Tung Tran,[ae] Ngoc Phuong Thuy Tran, [ae] Thi My Linh Phan, [ae] Huu An Ho, [ae] Tri Hieu Pham, [ae] Tuan Anh Luu,[be] Thi Quynh Anh Luong,[ce] Vu Uyen Nhi Nguyen[de] and Quoc Phu Phan *[ae]

Recently, the development of high-performance, low-cost materials with tunable redox properties has been of interest for advancing sustainable energy devices. In this study, nanocarbon (NC) particles derived from aniline and polyaniline-grafted nanocarbons (PANI-*g*-NC) were synthesized *via* a combination of solution plasma processing and a thermal reflux system. Compared with traditional catalysts, these PANI-*g*-NC hybrids offer distinct advantages: they avoid the high expense and limited availability of noble metals, provide higher electrical conductivity than pristine polymers, and introduce redox-active nitrogen functionalities that conventional carbons often lack. The solution plasma method enables the direct formation of nitrogen-doped nanocarbons from liquid aniline without the use of external templates. At the same time, the thermal reflux step ensures the efficient grafting of polyaniline chains onto the carbon surface. The obtained samples were characterized using advanced techniques, including SEM, TEM, Raman spectroscopy, XRD, and cyclic voltammetry (CV). SEM and TEM images revealed that the nanocarbon particles exhibit a spherical morphology. The FTIR spectra showed characteristic peaks corresponding to N–H stretching, aromatic C=C stretching, and C–N stretching in amines, confirming the successful grafting of polyaniline onto the nanocarbon surface. XRD analysis identified distinct diffraction peaks associated with multiple crystalline phases: nanocarbons (C), tungsten oxide (WO_3), and metallic tungsten (W). Meanwhile, electrochemical measurements (cyclic voltammetry) indicated a gradual decrease in the cyclic voltammetry loop area with increasing PANI grafting time. This study demonstrates an effective strategy to integrate the high electrical conductivity of nanocarbons with the redox activity of polyaniline *via* solution plasma processing, providing a green, sustainable, and low-cost platform for exploring charge-transfer mechanisms. More importantly, the PANI-*g*-NC hybrids exhibit a distinctive electrochemical behavior compared to conventional nanocarbons or bare polyaniline. The synergistic combination of a conductive carbon backbone with redox-active nitrogen functionalities in PANI enables a hybrid charge-storage mechanism that simultaneously enhances electron transport, proton accessibility, and catalytic site density. This dual contribution underlines the novelty of the present material design and its promising potential as an efficient and durable electrocatalyst.

Received 13th February 2026,
Accepted 7th March 2026

DOI: 10.1039/d6ma00205f

rsc.li/materials-advances

[a] *Department of Polymer Materials, Faculty of Materials Technology, Ho Chi Minh City University of Technology (HCMUT), Dien Hong Ward, 268 Ly Thuong Kiet Street, Ho Chi Minh City, Vietnam. E-mail: hung.nguyenbkidnet111@hcmut.edu.vn, nthuy.sdh241@hcmut.edu.vn, nbaduy.sdh241@hcmut.edu.vn, linh.trancamlinh12@hcmut.edu.vn, tung.tran.129k19@hcmut.edu.vn, thuy.tranktvl342@hcmut.edu.vn, linh.phanmylinhmybk@hcmut.edu.vn, an.ho2112729@hcmut.edu.vn, hieu.pham24062003@hcmut.edu.vn, pqphu@hcmut.edu.vn*

[b] *Department of Energy Materials and Applications, Faculty of Materials Technology, Ho Chi Minh City University of Technology (HCMUT), 268 Ly Thuong Kiet Street, Dien Hong Ward, Ho Chi Minh City, Vietnam. E-mail: luutuananh@hcmut.edu.vn*

[c] *Department of Metallurgy and Alloy Materials, Faculty of Materials Technology, Ho Chi Minh City University of Technology (HCMUT), 268 Ly Thuong Kiet Street, Dien Hong Ward, Ho Chi Minh City, Vietnam. E-mail: ltqanh@hcmut.edu.vn*

[d] *Department of Silicate Materials, Faculty of Materials Technology, Ho Chi Minh City University of Technology (HCMUT), 268 Ly Thuong Kiet Street, Dien Hong Ward, Ho Chi Minh City, Vietnam. E-mail: nvunhi@hcmut.edu.vn*

[e] *Vietnam National University Ho Chi Minh City (VNUHCM), Thu Duc Ward, Ho Chi Minh City, VietNam*

† Equal contributors.

Introduction

Global energy demand has risen sharply over the past three decades, driven by globalization, rapid urbanization, and the proliferation of electronic devices.[1] This growing demand has accelerated the search for sustainable and decentralized power solutions, prompting a shift toward clean energy technologies that mitigate environmental degradation and reduce reliance on fossil fuels. The global energy harvesting system market, valued at USD 1.0 billion in 2023, is projected to reach USD 3.0 billion by 2032 at a CAGR of 13.1%,[2] underscoring the urgency of developing efficient materials and systems to capture ambient energy from sources such as light, thermal gradients, and mechanical vibrations.[3,4] Within this broader context, materials that exhibit tunable redox properties and efficient charge transfer are central to advancing energy storage devices (*e.g.*, supercapacitors) and conversion technologies.[5,6] A key challenge in these systems is achieving high performance with abundant, inexpensive materials. Researchers are therefore turning to nanostructured carbon materials and conductive polymers as scalable alternatives, leveraging their physicochemical properties to enhance charge transfer and redox activity.[7] Nanocarbons (*e.g.*, graphene, carbon nanotubes, amorphous carbon) offer high surface area, excellent electrical conductivity, and robust durability, yet pure nanocarbons often lack sufficient active sites for efficient redox processes.[8–10] Nitrogen doping is known to introduce active nitrogenous sites (graphitic, pyridinic, and pyrrolic) that facilitate electron transfer and improve performance.[11–13] Building on this concept, conductive polymers such as polyaniline (PANI), which is inherently rich in nitrogen, can be grafted onto nanocarbons to provide synergistic benefits, including enhanced dispersion, interfacial stability, and additional redox-active sites.[14,15] PANI is particularly attractive due to its unique combination of properties: it possesses a highly conjugated structure with alternating single and double bonds, which facilitates electron mobility and charge transport along the polymer backbone.[16] This results in promising electrical conductivity, coupled with reversible redox activity, good electrocatalytic behavior, and high environmental and thermal stability.

This focus on metal-free, polymer-derived hybrid systems is well-supported by recent literature.[17] For instance, Sapner *et al.* demonstrated that L-lysine-functionalized reduced graphene oxide exhibits enhanced metal-free electrocatalytic properties for energy-related applications.[18] Furthermore, the integration of conducting polymers, such as polyaniline, with carbon nanostructures (*e.g.*, in PANI/MWCNT composites) has been shown to significantly enhance conductivity, stability, and overall electrochemical performance in energy harvesting and storage systems.[19,20]

However, to fully realize the potential of such hybrid architectures, the choice of synthesis method is critical. Conventional bottom-up techniques, including chemical vapor deposition (CVD), often demand high temperatures and vacuum environments, which not only raise energy consumption but also hinder large-scale production.[21] Meanwhile, top-down approaches such as mechanical milling involve repeated grinding, which can introduce impurities and compromise the integrity of nanostructures, thereby reducing catalytic efficiency.[22,23]

In this study, we employ solution plasma processing (SPP), an advanced technique that overcomes these limitations by simultaneously generating nanocarbon frameworks and activating aniline monomers directly in the liquid phase.[24,25] In this process, high-energy electrons and free radicals generated within the plasma play a critical role in initiating the chemical reactions. The mechanism begins when the plasma is ignited in the solvent, causing molecules near the electrode tips to vaporize or form bubbles due to Joule heating (producing solvent vapor) and electrolysis (generating gases such as H_2 and O_2). An electron avalanche is triggered inside these bubbles upon their formation. Electrical breakdown occurs within the bubbles, forming a plasma channel resembling a miniature lightning bolt.[26] This unbalanced discharge can be generated in various conductive liquids, where it functions to ionize species, accelerate ions, and multiply the initial seed electrons. Thus, the key stages of SPP can be summarized as follows: applying a high voltage induces bubble formation and electrical breakdown, resulting in unbalanced discharge plasma. This plasma subsequently establishes a unique reaction environment conducive to nanomaterial synthesis.[27]

This is followed by a reflux polymerization step, which facilitates the grafting of PANI onto the nanocarbons' surface through π–π stacking or covalent interactions.[28–32] Unlike conventional PANI/CNT or PANI/graphene hybrids that rely on expensive pre-synthesized carbon substrates and multi-step oxidative polymerization with external oxidants, this combined SPP-reflux strategy simultaneously achieves (i) *in situ* nitrogen doping of the carbon backbone, (ii) highly defective and reactive nanocarbon surfaces for stronger PANI anchoring, and (iii) partial covalent C–N grafting, all using only aniline as the sole carbon/nitrogen precursor and cheap tungsten electrodes. This subsequent treatment improves the interfacial compatibility and stability of the hybrid structure, ensuring more uniform polymer coverage on the nanocarbon framework.[33] The resulting nanocarbon–PANI hybrids combine the conductivity and surface area of nanocarbons with the nitrogen-rich catalytic properties of PANI, making them highly promising candidates for advanced energy applications, notably supercapacitors for energy storage and fuel cells for energy conversion.[34,35] By avoiding preformed carbon nanostructures and external oxidants, the present method offers a markedly simpler, lower-cost, and more scalable route compared to conventional PANI-grafted carbon hybrid materials. We anticipate that this material platform, with its demonstrated tunable redox activity and charge-transfer efficiency, may offer a promising foundation for future exploration in electrocatalytic applications, such as the oxygen reduction reaction.

Experimental procedure

Materials

Aniline (C_6H_7N, ≥99.5%) and acetone (C_3H_6O, ≥99.8%) were purchased from Sigma-Aldrich (St. Louis, MO, USA). Tungsten

rods (W, ≥99.95%, 3.0 mm in diameter and 200 mm in length) were obtained from Alfa Aesar (Ward Hill, MA, USA). All chemicals were of analytical grade and used without further purification.

Synthesis of the carbon material

For this experiment, a glass tube with open ends was used, with two tungsten electrodes positioned symmetrically at opposite ends. The electrodes were aligned face-to-face with a gap of less than 1 mm, carefully adjusted to avoid direct contact. Both electrodes were insulated and connected to the output terminals of a high-voltage module, which converted the input from a DC power supply (Vinasemi, 30 V–6 A) into a discharge voltage of approximately 1000–2000 V. Aniline solution was then introduced into the tube, and plasma discharge was initiated by switching on the power.

In the SPP process, plasma is generated between submerged electrodes using a bipolar-pulsed power supply, as illustrated in Fig. 1. Molecules in proximity to the electrodes are repeatedly struck by electrons emitted from the electrodes, thereby exciting and dissociating them. As a result, SPP induces the creation of numerous highly reactive chemical intermediates (*e.g.*, $^{\bullet}$CH, $^{\bullet}$CC, $^{\bullet}$CN, and $^{\bullet}C_6H_6$–NH_2 radicals) that drive a swift synthesis reaction for carbon nanomaterials.[35] The nitrogen atoms from the aniline solvent are incorporated into the graphitic lattice through a mechanism involving the reactive $^{\bullet}$CN radicals, which facilitate the formation of pyridinic (N at the edge of graphene layers, contributing lone-pair electrons) and graphitic (N substituting carbon within the graphene plane, altering electronic properties) nitrogen configurations.[36] This integration enhances the carbon framework with nitrogen-doped sites, promoting the rapid formation of functionalized nanocarbons rich in active groups suitable for catalytic applications.[36–38]

After 30 minutes of continuous plasma discharge, the generated nanocarbon products were collected by vacuum filtration through a nylon membrane filter (pore size: 0.22 μm). To remove residual organic molecules and by-products, the filtered solids were repeatedly washed with acetone until the filtrate became clear. The obtained carbon powder was subsequently dried in a convection oven at 200 °C for one hour to ensure complete removal of solvent traces and moisture. This final product, denoted as the nanocarbons without any polyaniline grafting, was labeled as NC (where 'NC' stands for nanocarbons). The sample was preserved in tightly sealed amber glass bottles under ambient conditions to prevent contamination and moisture absorption before further characterization. A schematic diagram illustrating the overall synthesis process of NC is provided in Fig. 2.

Synthesis of the polyaniline-grafted nanocarbon material

The synthesis of polyaniline-grafted nanocarbon materials was performed in two steps. Initially, nanocarbon materials were synthesized *via* a solution plasma process for 30 minutes. Subsequently, the obtained nanocarbon suspension was subjected to thermal grafting *via* reflux boiling at 180 °C. To investigate the influence of reaction time on grafting efficiency, two distinct timeframes were employed: 3 hours and 6 hours, while maintaining constant temperature and pressure. During the heating stage, radicals formed from the aniline solvent and the plasma-activated nanocarbon surface initiate the grafting process. These radicals, including phenyl and amine-derived species, facilitate the covalent attachment of aniline units to the nanocarbon surface *via* radical coupling, thereby forming initial aniline-grafted intermediates. As the reaction progresses, additional radicals form, driven by thermal energy and prolonged exposure, leading to chain propagation in which aniline monomers polymerize into PANI chains.[39,40] The proposed synthesis pathway of PANI-*g*-NC-H*x* is illustrated in Fig. 3. Here, the synthesized samples are denoted as PANI-*g*-NC-H*x*, where 'PANI-*g*-NC' denotes polyaniline-grafted nanocarbons and 'H*x*' denotes the reflux duration in hours (x = 3 or 6).

After heating, the products were collected and purified using the same filtration and washing procedures described above. The nanocarbon powders were then dried in an oven at 200 °C

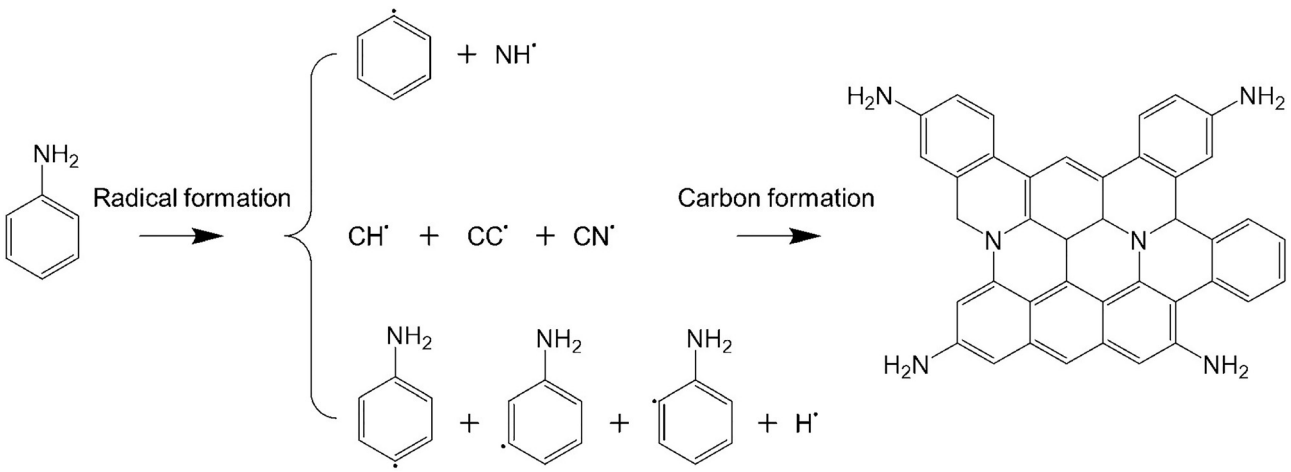

Fig. 1 Proposed formation mechanism of nanocarbon particles during the solution plasma process, illustrating plasma-induced precursor fragmentation and subsequent nucleation and growth of nitrogen-doped carbon domains.

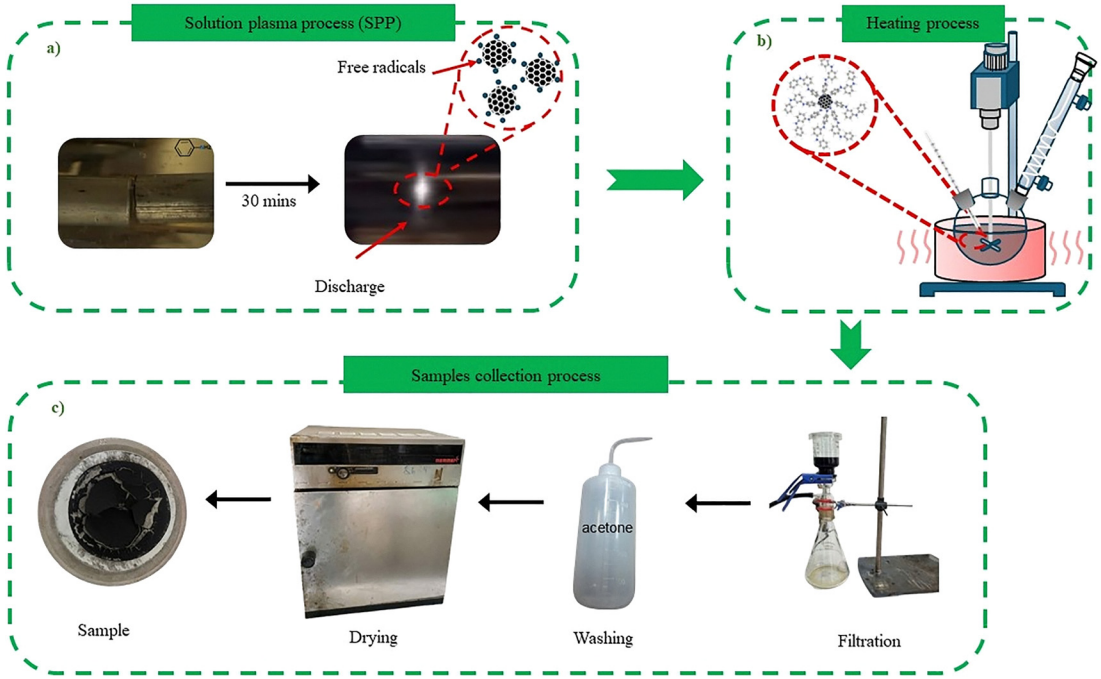

Fig. 2 Schematic representation of the synthetic strategy for NC (a and c) and PANI-*g*-NC-H*x* (a–c), combining plasma-derived nanocarbon formation with controlled thermal grafting to tailor the interfacial architecture.

for 1 h. The final products were designated as PANI-*g*-NC-H*x* and stored in sealed bottles at room temperature.

Material characterization

Scanning electron microscopy (SEM). The surface morphology of the synthesized NC and polyaniline-grafted nanocarbon was characterized using scanning electron microscopy (SEM) on a Hitachi S-4500 (Japan).

Transmission electron microscopy (TEM). Transmission electron microscopy (TEM) using a JEOL JEM-1400 (Japan) operated at an accelerating voltage of 200 kV was employed to investigate the internal nanostructure.

Fourier transform infrared spectroscopy (FTIR). The chemical structure of the nanocarbon and polyaniline-grafted nanocarbon was analyzed using Fourier transform infrared spectroscopy (FTIR) with a Thermo Nicolet 6700 (USA). Spectra were recorded in the range of 500–4000 cm^{-1} with a resolution of 2 cm^{-1} by averaging 64 scans.

X-ray diffraction (XRD). The crystallinity of the samples was examined by X-ray diffraction (XRD, Malvern Panalytical B.V., Netherlands) using CuKα radiation (λ = 0.154 nm) in the 2θ range of 10–80°.

Raman spectroscopy

Raman spectroscopy was performed using an XploRA ONE™ spectrometer (Horiba Scientific, Japan) in the spectral range of 1000–3500 cm^{-1} to analyze the structural order and disorder in the carbon-based samples. The intensity ratio of the D and G bands (I_D/I_G) was used to assess structural defects and the degree of graphitization.

Cyclic voltammetry (CV)

To quantify the electrochemical characteristics of the samples, cyclic voltammetry (CV) was performed using a Biologic MPG2 system. The experiment used a standard three-electrode cell setup, with a glassy carbon electrode (3 mm in diameter) as the working electrode, nickel foil as the counter electrode, and an Ag/AgCl electrode as the reference. The working electrode was fabricated by coating a slurry onto the glassy carbon substrate. The slurry contained a homogeneous mixture of the active material (70 wt%), carbon black C65 (15 wt%) as a conductive additive, and carboxymethyl cellulose (15 wt%) as a binder. The electrochemical behavior was assessed in a 0.5 M H_2SO_4 solution by scanning the potential from 0.0 to 1.4 V (*vs.* RHE) at a rate of 50 mV s^{-1} at room temperature.[41,42]

Results and discussion

Scanning electron microscopy (SEM)

These SEM images (Fig. 4) provide compelling visual evidence of morphological transformations resulting from the grafting of aniline onto nanocarbons. For the NC sample (Fig. 4a and b), the nanocarbons exhibit a spherical morphology with a pronounced tendency to aggregate into large clusters. This behavior is a direct consequence of strong van der Waals interactions among the particles, which overwhelm the weak electrostatic repulsive forces, thereby hindering effective dispersion. Consequently, the accessible surface area is significantly diminished.[43]

Upon subjecting the nanocarbons to aniline grafting, a marked alteration in morphology is observed. The particles

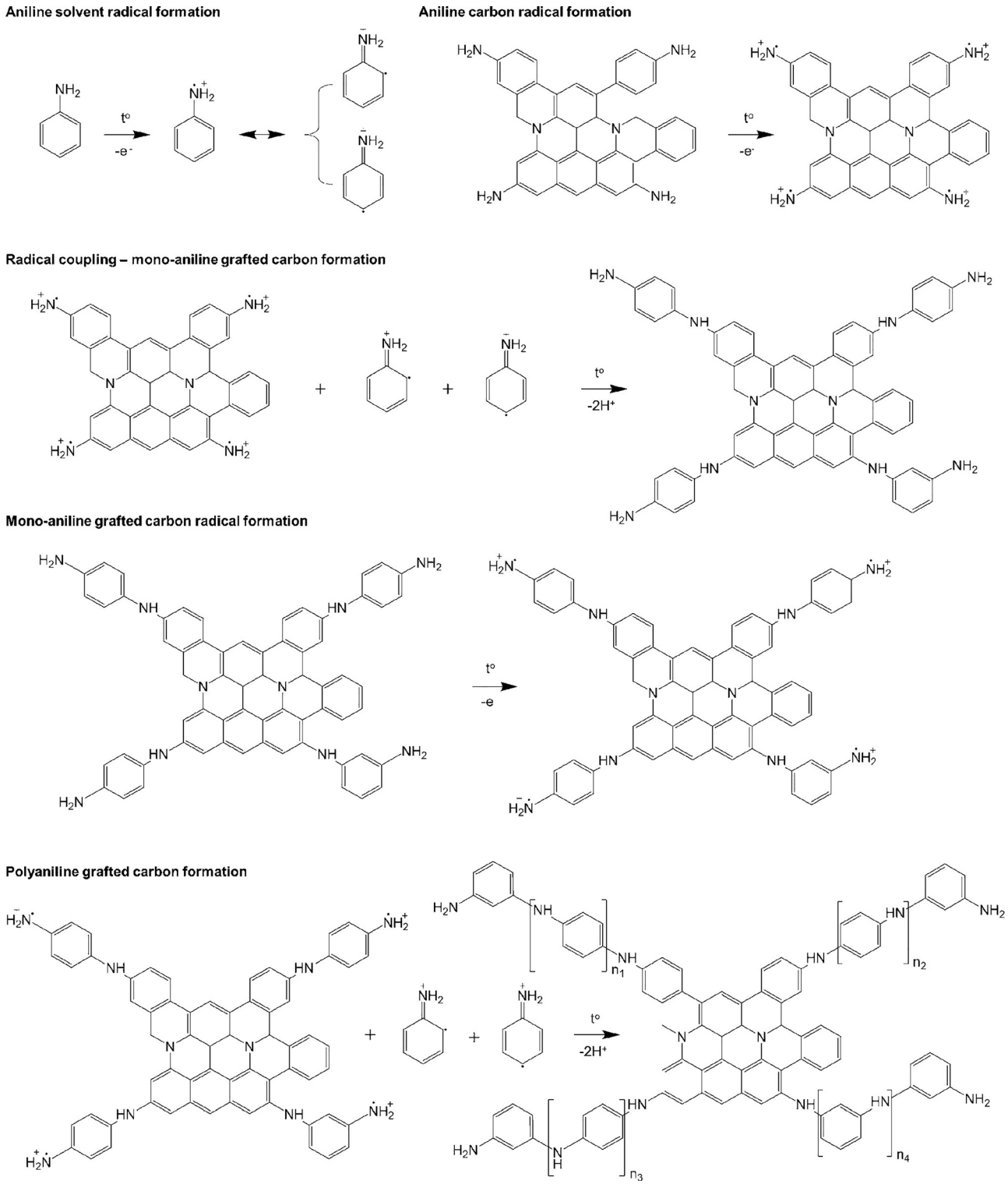

Fig. 3 Proposed interfacial grafting mechanism for polyaniline functionalization of nanocarbons during thermal treatment, involving surface radical activation and polymer chain propagation.

no longer form extensive aggregates but are instead uniformly distributed within a polymeric matrix. In the PANI-*g*-NC-H3 sample (Fig. 4c and d), the original particle shapes remain partially discernible, though numerous surface regions are coated with a thin polymeric layer. This indicates the initial adhesion of aniline onto the nanocarbons, thereby blurring particle boundaries and mitigating localized aggregation.

For the PANI-*g*-NC-H6 sample (Fig. 4e and f), the surface coverage is notably enhanced, with the PANI layer developing into a continuous network that separates the particles and

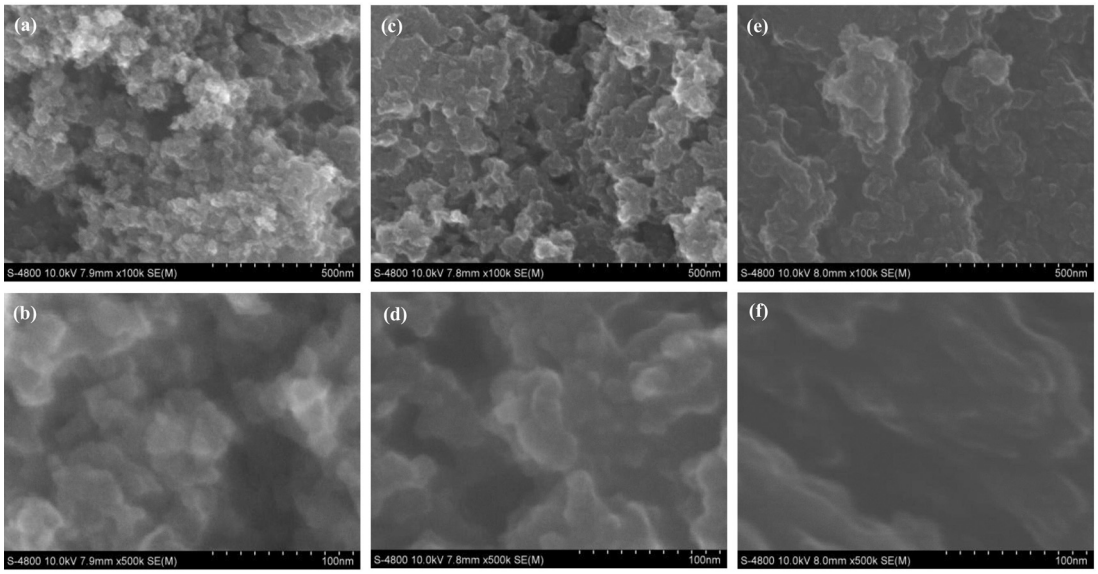

Fig. 4 SEM images of NC (a and b), PANI-*g*-NC-H3 (c and d), and PANI-*g*-NC-H6 (e and f), demonstrating progressive polymer coverage and reduced aggregation with increasing grafting duration.

reduces direct adsorptive interactions. This outcome underscores reaction time as a critical parameter influencing the thickness and continuity of the polymeric coating. Such a trend aligns with findings by Phan on polybenzene-carbon systems,[44] where extended reaction durations similarly facilitated the formation of a more complete coating.

These SEM results provide detailed insights into the morphological characteristics of the samples, including particle shape, aggregation tendencies, dispersion behavior, and the influence of reaction time, enabling a comprehensive understanding of how aniline grafting modifies the nanostructure of nanocarbons.

Transmission electron microscopy (TEM). These TEM images (Fig. 5) offer a detailed, high-resolution view of the internal makeup and boundary features of nanocarbons, both in their original state and after aniline grafting. For the NC sample (Fig. 5a), the nanocarbons show a mostly amorphous core with uneven edges and a tightly packed arrangement, in which individual particles join at contact points, highlighting clustering among them. The observed morphology at approximately 50 nm further confirms the nanoscale dimensions of the carbon domains, consistent with the expected particle size range for disordered nanocarbons.

With aniline grafting, TEM reveals a striking transformation into a hairy nanoparticle structure. In the PANI-*g*-NC-H3 sample (Fig. 5b), the nanocarbon cores are adorned with short, sparse polymeric protrusions, suggesting the initial growth of aniline-derived chains. This hairy layer, though limited, begins to disrupt the dense packing observed in NC, indicating early polymer attachment.[45]

For the PANI-*g*-NC-H6 sample (Fig. 5c), TEM shows a more pronounced hairy morphology, with longer and denser polymeric bristles extending from the nanocarbon surfaces. This enhanced growth, likely driven by extended radical coupling during reflux, creates a bristled appearance that further separates the particles, reducing direct contact. This aligns with trends observed in related polymer-nanocarbon systems, in which prolonged reaction times enhance surface modification.

These TEM images offer detailed insights into the internal structural characteristics, including the transition from

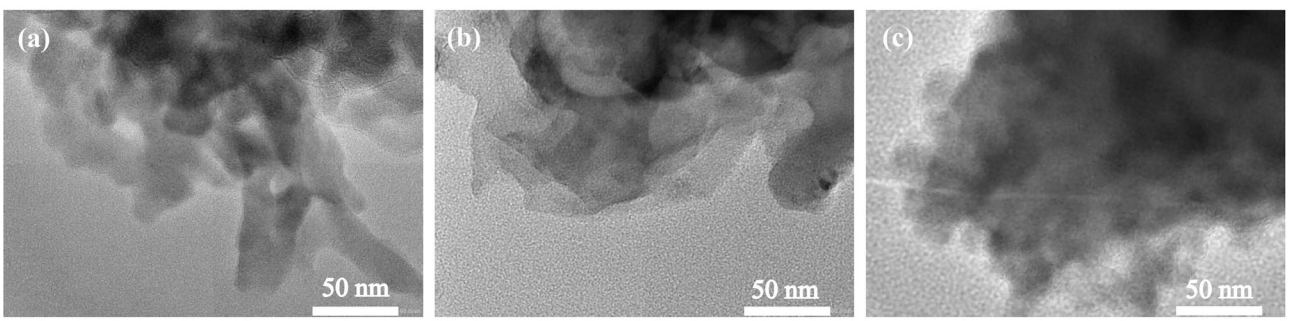

Fig. 5 TEM images of NC (a), PANI-*g*-NC-H3 (b), and PANI-*g*-NC-H6 (c), confirming the evolution from bare nanocarbon particles to core–shell architectures after polyaniline grafting.

amorphous cores to hairy nanoparticle structures, the density and length of polymeric protrusions, and the influence of reaction time, providing a clearer understanding of how aniline grafting alters the nanocarbon surface topology.

Raman spectroscopy

Raman spectroscopy was employed as a rapid and non-destructive tool to probe the structural evolution of the synthesized nanocarbon materials. In the Raman spectra, the D peak (around 1350 cm^{-1}) indicates the presence of defects or disorder in the carbon lattice, such as edges or sp^3-hybridized carbon, while the G peak (around 1580 cm^{-1}) reflects the in-plane stretching of sp^2-hybridized carbon atoms, representing the graphitic structure's integrity. The 2D peak (around 2700 cm^{-1}) provides insight into the stacking order and layer thickness of graphitic materials, with its shape and intensity offering clues about the material's crystallinity. The intensity ratio of the D to G peak (I_D/I_G) is a key metric: a higher ratio indicates increased disorder or defect density. In comparison, a lower ratio indicates a more ordered graphitic structure. As shown in Fig. 6, the sample NC exhibits pronounced D and G bands, with the D band being more intense. The corresponding I_D/I_G ratio of 1.11 suggests a considerable degree of disorder, most likely arising from synthesis-related defects, while the 2D band appears weak and poorly defined. For the PANI-*g*-NC-H3 sample, the D band remains dominant, and the I_D/I_G ratio increases to 1.24, indicating a higher level of disorder, which can be attributed to the initial attachment of PANI. The interaction, possibly through π–π stacking or partial covalent bonding, perturbs the graphitic lattice, while the 2D band shows no significant enhancement at this stage. A more pronounced structural transformation is observed in the 6-hour refluxed sample PANI-*g*-NC-H6, where both the D and G bands broaden and lose intensity, while the I_D/I_G ratio decreases substantially to 0.59. This reduction implies a lower degree of disorder, likely due to more extensive PANI polymerization that stabilizes the carbon framework. Nevertheless, the weaker signal intensity also suggests that excessive PANI may mask the Raman response of the nanocarbon. In contrast, the 2D band emerges more distinctly, albeit slightly broadened, indicating improved ordering accompanied by some structural heterogeneity. Overall, these results indicate that grafting duration critically influences the carbon structure: short reflux promotes lattice disruption, whereas prolonged treatment enhances structural order, although the Raman signal becomes increasingly affected by the polymer coating.

Fourier-transform infrared spectroscopy (FTIR). The FTIR spectra in Fig. 7 reveal the evolution of functional groups across the synthesized materials, with the NC and PANI-*g*-NC-H3 samples showing minimal differences, both exhibiting a weak, broad peak at 3450 cm^{-1} due to O–H stretching from adsorbed water or surface hydroxyl groups on the nanocarbons, with no significant peaks at 794 cm^{-1} (out-of-plane C–H bending) or 1078 cm^{-1} (C–O stretching), indicating negligible PANI presence in these samples. This lack of characteristic PANI peaks indicates that the 3-hour grafting period (PANI-*g*-NC-H3) is insufficient for substantial polymer formation, with the spectra dominated by the native nanocarbon surface chemistry. In contrast, the PANI-*g*-NC-H6 sample displays a marked transformation, with a stronger, broader 3450 cm^{-1} peak dominated by N–H stretching from PANI's amine groups and a minor O–H contribution from trapped moisture, alongside newly intensified peaks at 794 cm^{-1} (out-of-plane C–H bending in benzenoid rings) and 1078 cm^{-1} (C–O stretching, likely from PANI oxidation or surface interactions), highlighting that prolonged grafting significantly enhances PANI formation and coverage compared to the nearly unchanged NC and PANI-*g*-NC-H3 samples. Specifically, the 794 cm^{-1} peak, a hallmark of the aromatic C–H out-of-plane bending in PANI's benzenoid structure, becomes prominent due to the increased density of polymer chains formed during the extended 6-hour reflux, reflecting enhanced polymerization and structural ordering of the benzenoid units. The 1078 cm^{-1} peak, indicative of C–O

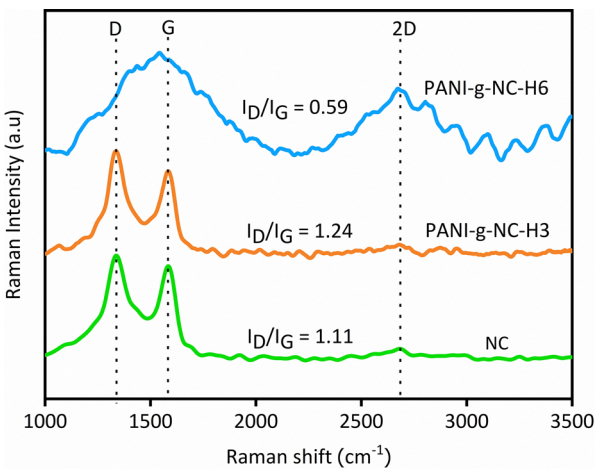

Fig. 6 Raman spectra of NC, PANI-*g*-NC-H3, and PANI-*g*-NC-H6, showing modulation of the I_D/I_G ratio and structural disorder upon grafting.

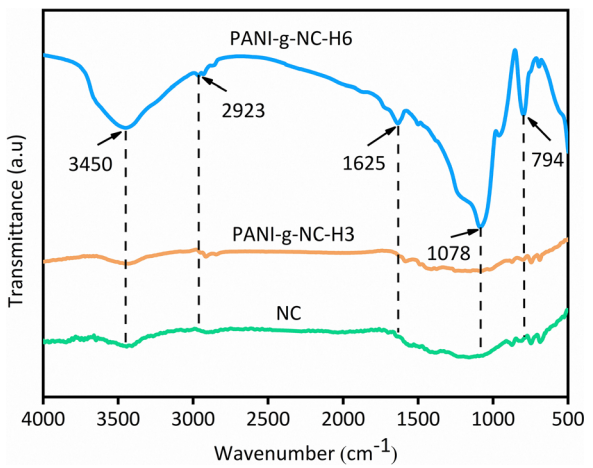

Fig. 7 FTIR spectra of NC, PANI-*g*-NC-H3, and PANI-*g*-NC-H6, confirming successful incorporation of polyaniline through characteristic quinoid and benzenoid vibrations.

stretching, likely arises from oxidative side reactions during grafting or interactions between PANI and the nanocarbon surface, such as the formation of ether linkages or oxygen-containing groups, which are more pronounced with longer reaction times as PANI coverage thickens and interacts more extensively with the substrate. These spectral changes underscore the effectiveness of prolonged grafting in achieving a robust PANI layer, potentially boosting the material's electrocatalytic properties. Overall, the FTIR analysis concludes that PANI is successfully grafted onto nanocarbons, evidenced by the emergence of N–H, C–H, and C–O related peaks in the PANI-*g*-NC-H6 sample, suggesting a more effective functionalization that could improve the material's electrocatalytic properties. At the same time, the minimal changes in NC and PANI-*g*-NC-H3 indicate limited PANI grafting under shorter reaction times.

X-ray diffraction analysis (XRD). The XRD patterns of the three samples, as depicted in Fig. 8, reveal varying degrees of crystallinity and the presence of metallic impurities. Characteristic peaks observed at 2θ values of approximately 26° and 43° are assigned to carbon phases (C). The diffraction peaks positioned at 2θ values of around 39°, 46°, 62°, and 72° are indexed to tungsten carbide (WC, WC_2). Furthermore, peaks appearing at 2θ values of about 25°, 29°, and 40° correspond to tungsten oxide (WO_3), while signals centered at 2θ values of roughly 57° and 74° are characteristic of metallic tungsten (W). The ungrafted NC sample shows WO_3 peaks slightly more intense than carbon, reflecting greater oxidation of tungsten residues in the absence of PANI protection. At the same time, the W intensity is comparable to that of carbon, suggesting balanced contributions from metallic and amorphous carbon due to incomplete carburization. In the PANI-*g*-NC-H3 sample, carbon and tungsten peaks intensify modestly while WO_3 decreases, indicating a more balanced structure where partial PANI coverage reduces oxidation reactions (less WO_3 generation) by shielding tungsten species, thus limiting further oxide formation during the process. For the PANI-*g*-NC-H6 sample, the intensities of carbon, tungsten, and tungsten oxide peaks rise overall, with the WO_3 peak becoming broader and less sharp compared to the sharper, higher WO_3 in NC and PANI-*g*-NC-H3, possibly due to prolonged grafting inducing strain or disorder in the WO_3 lattice from denser PANI encapsulation. At the same time, the increased coverage enhances interfacial interactions but may mask some crystalline signals. Such extended grafting time appears to stabilize phases and reduce susceptibility to oxidation, though the broader WO_3 peaks indicate smaller crystallite sizes or increased amorphous contributions. In summary, the XRD results highlight that grafting with PANI not only modulates the relative intensities of carbon, tungsten, and tungsten oxide phases but also suppresses the diffraction peak intensities through polymer coverage, which shields tungsten species from excessive oxidation, thereby enhancing the structural stability of the nanocarbon materials. Although tungsten and other tungsten species are present, their low concentration and dispersion, largely masked by other carbon nanoparticles, do not negatively affect the material's overall performance. Previous studies have also confirmed this.[36,46]

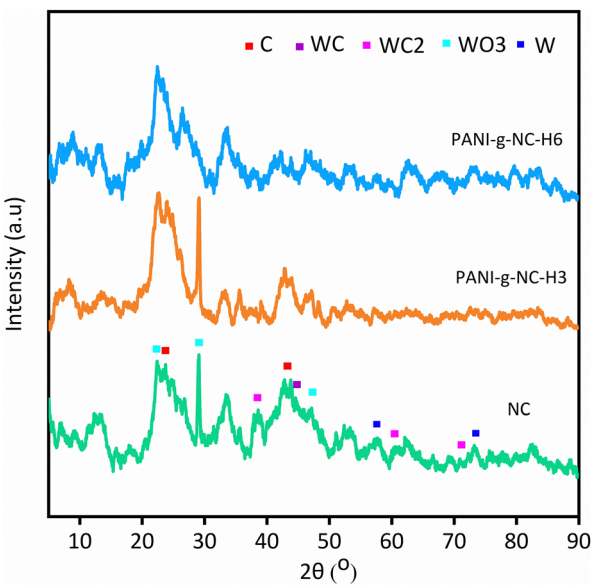

Fig. 8 XRD patterns of NC, PANI-*g*-NC-H3, and PANI-*g*-NC-H6, revealing attenuation of graphitic reflections due to polymer coating and interfacial modification.

Cyclic voltammetry (CV)

Cyclic voltammetry measurements were conducted in 0.5 N H_2SO_4 electrolyte at a scan rate of 50 mV s^{-1}, as shown in Fig. 9. The nanocarbons (NC) display the highest current response, which can be attributed to their large accessible surface area and high density of electroactive sites. This suggests efficient adsorption–desorption of protons (hydrogen ions) at the nanocarbon interface, a fundamental requirement for electrocatalytic processes.

When polyaniline is grafted, as in PANI-*g*-NC-H3 and PANI-*g*-NC-H6, the enclosed CV area decreases progressively from NC to PANI-*g*-NC-H6, indicating that polymer coverage partially blocks active carbon sites and reduces the overall capacitive response. However, the presence of nitrogen functionalities within the PANI chains introduces a different mechanism: the redox-active amine groups engage in proton-coupled electron transfer (PCET), which manifests as distinct anodic and cathodic peaks.[47] PCET is a well-established mechanism in electrocatalysis that involves the concerted or sequential transfer of an electron and a proton between the electrode (material) and the electrolyte, which is crucial for lowering activation barriers in redox reactions.[48] Conjugated polymers and nitrogen-doped nanocarbon systems have been shown to facilitate PCET by providing both protonation sites and efficient electron conduction pathways.[49,50] For example, in a conjugated multiredox polymer system, super-Nernstian PCET behavior was observed, underscoring the ability of polymer backbones to support rich proton–electron coupling.[50] In the PANI-*g*-NC-H*x* system, grafted PANI introduces nitrogen sites (–NH, =N–) that can act as protonation centers, while its extended π-conjugated backbone provides an efficient electron pathway. Together, these features establish favorable conditions for PCET at the hybrid

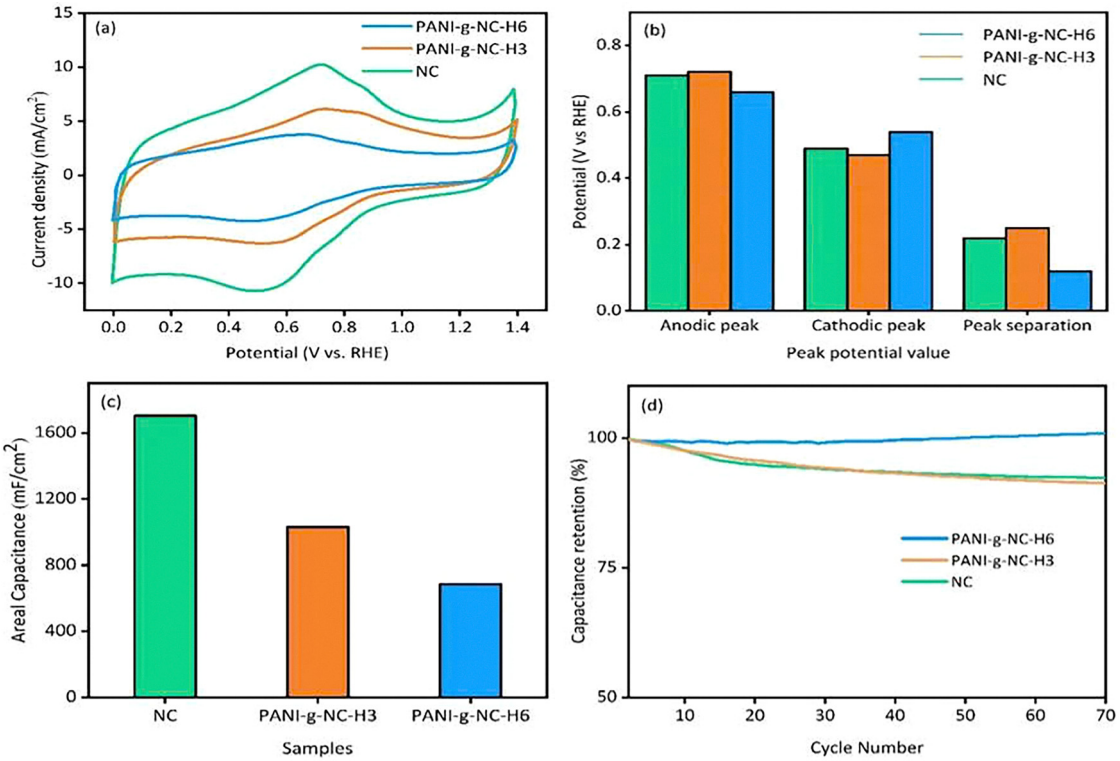

Fig. 9 Electrochemical performance of the fabricated electrodes in 0.5 N H_2SO_4 at 50 mV s^{-1}, including cyclic voltammetry (a), peak potential separation (b), areal capacitance (c), and capacitance retention (d), demonstrating enhanced proton coupled electron transfer kinetics after grafting.

interface. Moreover, the hybrids benefit from strong proton–π interactions between electrolyte H^+ ions and the electron-rich conjugated domains as well as heteroatomic sites of polyaniline. These interactions not only enable localized charge storage and highly reversible redox cycling,[51] but also help stabilize the electrochemical interface and promote efficient electron transport across the network.

Comparing PANI-*g*-NC-H3 and PANI-*g*-NC-H6, the peak-to-peak separation (ΔE_p) is larger for PANI-*g*-NC-H3, indicating slower reversibility of electron transfer at moderate grafting levels. In this case, charge carriers are temporarily trapped within the polymer backbone before returning to the carbon network, which limits the rate of catalytic redox reactions. By contrast, PANI-*g*-NC-H6 shows a smaller ΔE_p, reflecting faster redox dynamics that enhance its ability to mediate proton-coupled electron transfer. To deeply understand the kinetics of the proton-coupled electron transfer mechanism, the peak potential separation (ΔE_p) between the anodic (E_{pa}) and cathodic (E_{pc}) peaks was analyzed. According to the mechanistic framework established by Huynh and Meyer (*Chem. Rev.* 2007)[48] and Costentin (*Chem. Rev.* 2008),[52] the magnitude of ΔE_p serves as a critical diagnostic for the reversibility and the rate of the coupled proton–electron transfer.[9]

$$\Delta E_p = E_{pa} - E_{pc}$$

In the PANI-*g*-NC-H6 hybrid, the CV curves exhibit a well-defined redox pair with a peak separation of approximately 120 mV (at 10 mV s^{-1}). This relatively narrow ΔE_p indicates that the electron transfer is tightly coupled with protonation/deprotonation at the nitrogen sites (–NH–/–N═) without significant kinetic barriers. If the proton transfer were sluggish or decoupled (stepwise mechanism), a larger overpotential would be required to drive the reaction, resulting in a significantly widened ΔE_p. Therefore, the observed small peak separation confirms a concerted or synchronous PCET pathway, in which the PANI matrix facilitates rapid proton transport to compensate for the electron flow, ensuring high reversibility and structural stability during cycling.

Although the higher coverage in PANI-*g*-NC-H6 lowers the current density due to reduced exposure of active carbon domains, the continuous PANI coating effectively bridges the originally discrete nanocarbon particles, thereby improving electronic connectivity across the electrode. This enhancement in conductivity offsets the shielding effect of polymer coverage and directly improves electrocatalytic efficiency by accelerating charge transfer between the conjugated backbone and the electrolyte. Meanwhile, NC, with its broad CV envelope and weak redox features, remains governed by surface-controlled adsorption–desorption rather than true PCET. The poor electrical connectivity between isolated nanocarbon particles explains why its redox peaks are indistinct despite the large overall current response.

The cycling stability of the modified supercapacitor electrodes was also investigated. The electrodes were subjected to 70 continuous CV cycles at a scan rate of 50 mV s^{-1} in 0.5 N H_2SO_4

aqueous electrolyte at room temperature to assess their durability (Fig. 9). Both PANI-*g*-NC-H3 and PANI-*g*-NC-H6 exhibit enhanced capacitance retention compared to NC. For PANI-*g*-NC-H6, a gradual increase in capacitance is observed throughout the cycling test. This behavior can be explained by the progressive intercalation of protons into the well-structured polyaniline backbone, thereby forming stable proton–π pairs. Upon repeated charge–discharge, the improved electronic conductivity of the PANI network, developed over 6 hours, enables efficient electron transport during the redox process, which in turn facilitates the release and reinsertion of H^+ ions between the electrode and electrolyte. As a result, the system quickly reaches equilibrium and maintains a stable capacitance response, highlighting the promising durability of PANI-*g*-NC-H6. In contrast, the PANI-*g*-NC-H3 electrode also shows higher retention than bare NC, but the stability enhancement is less pronounced. The lower degree of polymer coverage after only 3 hours of grafting leaves parts of the nanocarbon framework insufficiently connected, thereby restricting electron transport. This incomplete conductivity traps some protons within the structure, limiting full reversibility during cycling. Consequently, although PANI-*g*-NC-H3 mitigates the degradation issues of bare NC due to the nitrogen functionalities introduced by PANI, its long-term stability still lags behind that of PANI-*g*-NC-H6.

Building on the insights from the cyclic voltammetry analysis, which highlighted the enhanced charge-transfer kinetics and conductivity in PANI-grafted nanocarbons, the conductivity mechanism can be further elucidated (Fig. 10). The conductivity phenomenon in nanocarbons primarily occurs at contact zones, or touchpoints, where individual carbon particles meet.[53,54] At these interfaces, electron transport is facilitated through direct overlap of π-orbitals from adjacent sp^2-hybridized carbon atoms, enabling efficient charge transfer when the particles are in physical contact.[55] This touching-point conductivity is critical because it allows electrons to move between discrete nanocarbon domains. On the other hand, grafting PANI onto nanocarbons significantly enhances the overall conductivity of the hybrid system, acting as a conductive bridge that interconnects the nanocarbon particles. This improvement stems from PANI's role as an electrically conductive polymer, whose extended π-conjugated backbone serves as a "wiring" network, linking the originally isolated nanocarbons

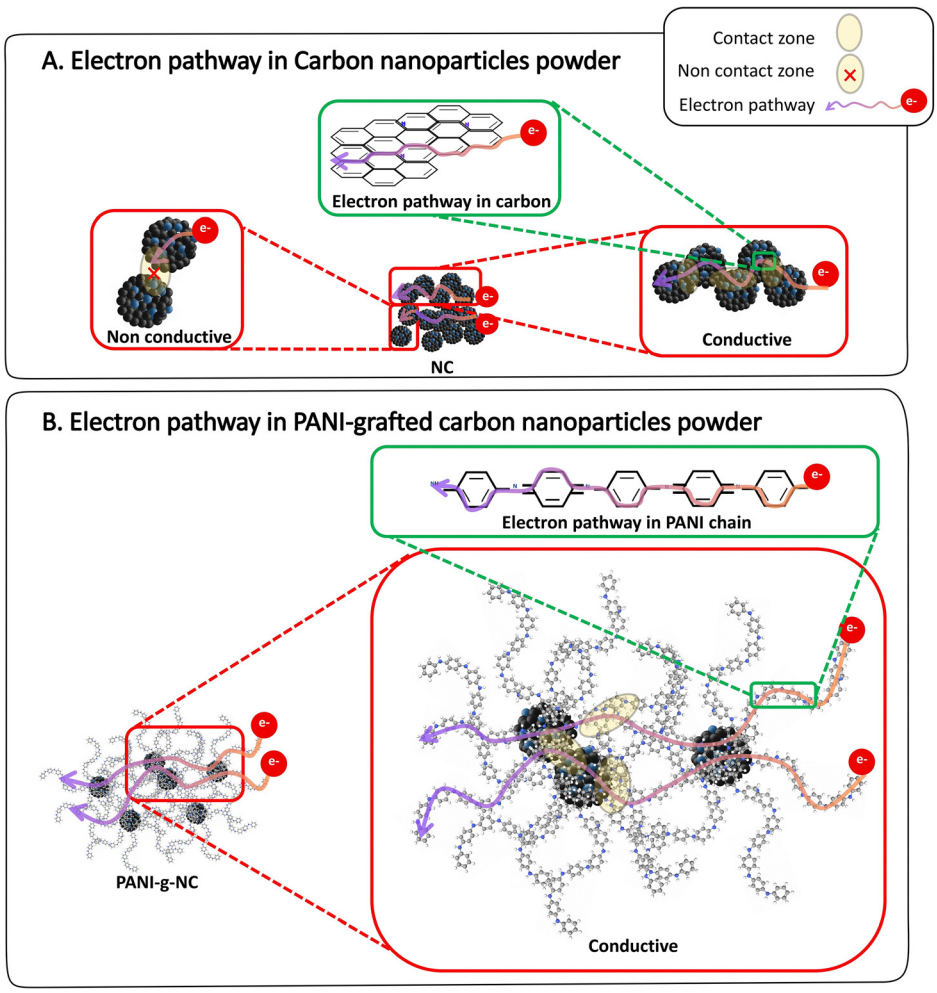

Fig. 10 Schematic illustration of the interconnected conductive network in (A) non-bridged nanocarbons (NCs) and (B) PANI-*g*-NC, highlighting improved electron and ion transport pathways in the nanoparticle (NC) powder.

into a more cohesive conductive framework. The conductivity mechanism involves three key interaction types: (i) PANI chain-to-PANI chain interactions; (ii) PANI chain-to-nanocarbon interactions, where covalent bonds or π–π interactions at the graft interface facilitate electron transfer from the carbon surface to the polymer, boosting interfacial conductivity; (iii) nanocarbon-to-nanocarbon interactions, which are preserved and augmented by the PANI coating that bridges gaps between particles, reducing contact resistance. This proposed theory suggests that the PANI layer not only compensates for the limited connectivity of pristine nanocarbons, but also amplifies the hybrid system's electrocatalytic efficiency.

In conclusion, grafting polyaniline effectively shifts the electrochemical behavior of nanocarbon from simple surface-controlled proton adsorption to a more advanced hybrid proton-coupled electron transfer pathway. PANI-*g*-NC-H3 exhibits a higher current response and moderate enhancement in charge-transfer kinetics, but its improvements remain limited due to incomplete polymer coverage. In contrast, despite the extensive coverage of nanocarbon surfaces by polyaniline in PANI-*g*-NC-H6, the material still maintains efficient electron conduction and demonstrates remarkable stability over prolonged cycling. This balance of durability and electronic conductivity establishes PANI-*g*-NC-H6 as the most reliable and robust candidate among the investigated materials.

Overall, the findings highlight the pivotal role of grafting duration in optimizing electrocatalytic performance, with PANI-*g*-NC-H6's 6-hour grafting yielding promising charge-transfer kinetics, enhanced proton-coupled electron transfer, and around 90% capacitance retention over 80 cycles, thus providing a targeted pathway for developing cost-effective, durable catalysts tailored for the ORR in fuel cell applications.

Conclusions

This study successfully demonstrates the synthesis of nanocarbons grafted with polyaniline using a solution plasma technique. The properties of the resulting materials were effectively tuned by controlling the heating time during synthesis. The preliminary results indicate the promising potential of the PANI-*g*-NC hybrid material as a low-cost, environmentally friendly metal-free electrocatalyst for the oxygen reduction reaction (ORR) and supercapacitors, owing to its hybrid charge-storage mechanism and the synergistic effect between N-doped nanocarbons and grafted PANI. Grafting polyaniline onto the nanocarbon surface significantly enhances the material's electrical conductivity and charge-transport capability. Moreover, the ability to tailor the material's properties, balancing charge storage capacity with electrical conductivity, by simply varying the synthesis duration, provides a straightforward and powerful strategy for designing advanced materials. However, the current study is limited to qualitative cyclic voltammetry (CV) data obtained over a small number of cycles (70). It lacks in-depth ORR-specific evaluations, long-term durability assessments, and performance under realistic operating conditions. These limitations will be addressed in future studies when additional equipment resources and funding become available. This work establishes solution plasma processing as a versatile method for developing next-generation grafted nanomaterials for sustainable energy technologies.

Author contributions

Nguyen Tien Hung conceptualized the study, designed the methodology, supervised the work, and validated the results, and drafted the manuscript, including the Abstract, Introduction, Results, and Discussion (SEM, TEM, and Raman analyses), Graphical Abstract, and preparation of procedure images. Nguyen Thanh Huy curated data, performed analysis and visualization, and contributed to manuscript writing, and assisted in planning the work and revising the manuscript. Nguyen Bui Anh Duy performed formal analysis, participated in the investigation, and contributed to manuscript revision. Tran Thi Cam Linh conducted the experiments, including sample preparation and synthesis, and assisted with data analysis. Tran Thanh Tung performed experiments, processed measurements, and supported data interpretation. Tran Ngoc Phuong Thuy conducted FTIR and XRD analyses and assisted in data interpretation. Phan Thi My Linh contributed to writing the Experimental Procedure section and supported data analysis. Ho Huu An analyzed the cyclic voltammetry results. Pham Tri Hieu assisted in manuscript review. Luu Tuan Anh assisted with experimental design and carried out supporting measurements. Luong Thi Quynh Anh participated in preparing figures and revising the graphics of the manuscript. Nguyen Vu Uyen Nhi performed supporting experiments and contributed to manuscript review. Phan Quoc Phu supervised the project, developed the theoretical background, proposed the reaction mechanisms, and revised the manuscript.

Conflicts of interest

There are no conflicts to declare.

Data availability

All data that support the findings of this study are available from the corresponding author upon reasonable request. This includes the crucial experimental data for the synthesis and characterization of the compounds, as well as the raw data for the electrochemical measurements. Additionally, the computational methods and parameters used in this study, along with the input files and output data, are fully described and available.

Supplementary information (SI) provides comprehensive characterization data of the synthesized materials, including FTIR, Raman, and XRD spectra, along with the raw numerical data for the cyclic voltammetry (CV) measurements. These datasets support the structural analysis and electrochemical

performance discussed in the main manuscript. See DOI: https://doi.org/10.1039/d6ma00205f.

Acknowledgements

We acknowledge the Ho Chi Minh City University of Technology (HCMUT), VNU-HCM, for supporting this study.

References

1 P. Bajpai and V. Dash, Hybrid renewable energy systems for power generation in stand-alone applications: A review, *Renewable Sustainable Energy Rev.*, 2012, **16**, 2926–2939.
2 S. Research, Energy Harvesting System Market Size, *Share & Trends Report 2032*, https://straitsresearch.com/report/energy-harvesting-system-market, (accessed 12 February 2026).
3 W. Lu, W. L. Ong, X. Pan, Z. Li, G. Tian and G. W. Ho, Design Strategies and Roles of Hydrogels for Sustainable Energy Conversion and Harvesting from Natural and Biological Environments, *Adv. Mater.*, 2025, **37**, e10270.
4 M. Mohammadi and I. Sohn, AI based energy harvesting security methods: A survey, *ICT Express*, 2023, **9**, 1198–1208.
5 Y. Liu, N. Tian, X.-H. Liu and H. Shang, High-performance N-doped activated carbon derived from walnut green peel for supercapacitors, *Biomass Conv. Bioref.*, 2024, **14**, 14641–14651.
6 X. Chu, W. Yang and H. Li, Recent advances in polyaniline-based micro-supercapacitors, *Mater. Horiz.*, 2023, **10**, 670–697.
7 *Nanostructured Materials for Next-Generation Energy Storage and Conversion: Fuel Cells*, ed F. Li, S. Bashir and J. L. Liu, Springer, Berlin, Heidelberg, 2018.
8 Y. Ji, L. Huang, J. Hu, C. Streb and Y.-F. Song, Polyoxometalate-functionalized nanocarbonsmaterials for energy conversion, energy storage and sensor systems, *Energy Environ. Sci.*, 2015, **8**, 776–789.
9 Y. Liu, J. Zhang, Y. Cheng and S. P. Jiang, Effect of Carbon Nanotubes on Direct Electron Transfer and Electrocatalytic Activity of Immobilized Glucose Oxidase, *ACS Omega*, 2018, **3**, 667–676.
10 L.-H. Zhang, Y. Shi, Y. Wang and N. R. Shiju, NanocarbonsCatalysts: Recent Understanding Regarding the Active Sites, *Adv. Sci.*, 2020, **7**, 1902126.
11 H. Wang, T. Maiyalagan and X. Wang, Review on Recent Progress in Nitrogen-Doped Graphene: Synthesis, Characterization, and Its Potential Applications, *ACS Catal.*, 2012, **2**, 781–794.
12 J. Duan, S. Chen, M. Jaroniec and S. Z. Qiao, Heteroatom-Doped Graphene-Based Materials for Energy-Relevant Electrocatalytic Processes, *ACS Catal.*, 2015, **5**, 5207–5234.
13 Y. Shao, J. Sui, G. Yin and Y. Gao, Nitrogen-doped carbon nanostructures and their composites as catalytic materials for proton exchange membrane fuel cell, *Appl. Catal., B*, 2008, **79**, 89–99.
14 L. Qu, Y. Liu, J.-B. Baek and L. Dai, Nitrogen-doped graphene as efficient metal-free electrocatalyst for oxygen reduction in fuel cells, *ACS Nano*, 2010, **4**, 1321–1326.
15 A. Eftekhari, L. Li and Y. Yang, Polyaniline supercapacitors, *J. Power Sources*, 2017, **347**, 86–107.
16 R. A. Kale, S. C. Dhawale, B. B. Mulik, A. Adhikari and B. R. Sathe, Polyaniline based highly selective electrochemical sensor for ascorbic acid determination: Performance studies towards real sample analysis, *J. Ind. Eng. Chem.*, 2024, **136**, 167–176.
17 Q. Zhai, H. Huang, T. Lawson, Z. Xia, P. Giusto, M. Antonietti, M. Jaroniec, M. Chhowalla, J.-B. Baek, Y. Liu, S. Qiao and L. Dai, Recent Advances on Carbon-Based Metal-Free Electrocatalysts for Energy and Chemical Conversions, *Adv. Mater.*, 2024, **36**, 2405664.
18 V. S. Sapner, P. P. Chavan and B. R. Sathe, l-Lysine-Functionalized Reduced Graphene Oxide as a Highly Efficient Electrocatalyst for Enhanced Oxygen Evolution Reaction, *ACS Sustainable Chem. Eng.*, 2020, **8**, 5524–5533.
19 Z. Mustafa, R. K. Ghadai, B. B. Pradhan, B. P. Swain, J. Biswas and D. Kumar, Recent advances in polyaniline/graphene nanocomposites for supercapacitor applications: Synthesis, properties, and future directions, *Results Surf. Interfaces*, 2024, **17**, 100316.
20 R. Gangopadhyay, *Conducting Polymer–GO/RGO Nanocomposites: New Generation Hybrid Materials for Supercapacitor Applications*.
21 Y. M. Manawi, Ihsanullah, A. Samara, T. Al-Ansari and M. A. Atieh, A Review of Carbon Nanomaterials' Synthesis via the Chemical Vapor Deposition (CVD) Method, *Materials*, 2018, **11**(5), 822.
22 A. P. Amrute, J. De Bellis, M. Felderhoff and F. Schüth, Mechanochemical Synthesis of Catalytic Materials, *Chem. – Eur. J.*, 2021, **27**, 6819–6847.
23 N. Baig, I. Kammakakam and W. Falath, Nanomaterials: a review of synthesis methods, properties, recent progress, and challenges, *Mater. Adv.*, 2021, **2**, 1821–1871.
24 G. Panomsuwan, N. Saito and T. Ishizaki, Nitrogen-doped carbon nanoparticles derived from acrylonitrile plasma for electrochemical oxygen reduction, *Phys. Chem. Chem. Phys.*, 2015, **17**, 6227–6232.
25 N. Thongwichit, O. L. H. Li, W. Yaowarat, N. Saito and U. Suriyapraphadilok, Adsorption of carbon dioxide by solution-plasma-synthesized heteroatom-doped carbon nanospheres, *Jpn. J. Appl. Phys.*, 2015, **55**, 01AE10.
26 N. Saito, M. A. Bratescu and K. Hashimi, Solution plasma: A new reaction field for nanomaterials synthesis, *Jpn. J. Appl. Phys.*, 2017, **57**, 0102A4.
27 C. Chokradjaroen, J. Niu, G. Panomsuwan and N. Saito, Insight on Solution Plasma in Aqueous Solution and Their Application in Modification of Chitin and Chitosan, *Int. J. Mol. Sci.*, 2021, **22**(9), 4308.
28 Z. Wang, L. Jiang, Y. Wei and C. Zong, In-situ polymerization to prepare reduced graphene oxide/polyaniline composites for high performance supercapacitors, *J. Energy Storage*, 2020, **32**, 101742.

29 J. Li, S. Qiu, B. Liu, H. Chen, D. Xiao and H. Li, Strong interaction between polyaniline and carbon fibers for flexible supercapacitor electrode materials, *J. Power Sources*, 2021, **483**, 229219.
30 J.-E. Huang, X.-H. Li, J.-C. Xu and H.-L. Li, Well-dispersed single-walled carbon nanotube/polyaniline composite films, *Carbon*, 2003, **41**, 2731–2736.
31 Q. Jiang, Q. Zhang, X. Wu, L. Wu and J.-H. Lin, Exploring the Interfacial Phase and π–π Stacking in Aligned Carbon Nanotube/Polyimide Nanocomposites, *Nanomaterials*, 2020, **10**(6), 1158.
32 M. Yang, V. Koutsos and M. Zaiser, Interactions between Polymers and Carbon Nanotubes: A Molecular Dynamics Study, *J. Phys. Chem. B*, 2005, **109**, 10009–10014.
33 Q. Wang, J. Li, D. Wang, J. Niu, P. Du, J. Liu and P. Liu, Enhanced electrochemical performance of polyaniline-based electrode for supercapacitors in mixed aqueous electrolyte, *Electrochim. Acta*, 2020, **349**, 136348.
34 T. Pimklang, A. Watthanaphanit and P. Pakawatpanurut, Novel green synthesis of graphene oxide-manganese dioxide using solution plasma process for energy storage, *Chem. Eng. J.*, 2022, **442**, 136244.
35 L. Wang, X. Lu, S. Lei and Y. Song, Graphene-based polyaniline nanocomposites: preparation, properties and applications, *J. Mater. Chem. A*, 2014, **2**, 4491–4509.
36 D. Kim, O. L. Li, P. Pootawang and N. Saito, Solution plasma synthesis process of tungsten carbide on N-doped carbon nanocomposite with enhanced catalytic ORR activity and durability, *RSC Adv.*, 2014, **4**, 16813–16819.
37 J. Niu, C. Chokradjaroen, Y. Sawada, X. Wang and N. Saito, Plasma–Solution Junction for the Formation of Carbon Material, *Coatings*, 2022, **12**(11), 1607.
38 C. Chokradjaroen, X. Wang, J. Niu, T. Fan and N. Saito, Fundamentals of solution plasma for advanced materials synthesis, *Mater. Today Adv.*, 2022, **14**, 100244.
39 S. Zhou, G. M. Anderson, B. Mondal, E. Doni, V. Ironmonger, M. Kranz, T. Tuttle and J. A. Murphy, Organic super-electron-donors: initiators in transition metal-free haloarene–arene coupling, *Chem. Sci.*, 2013, **5**, 476–482.
40 A. Studer and D. P. Curran, Organocatalysis and C-H activation meet radical- and electron-transfer reactions, *Angew. Chem., Int. Ed.*, 2011, **50**, 5018–5022.
41 S. Kornnum, P. Chomkhuntod, N. Schwaiger, K. Limcharoen, K. Deshsorn, K. Jitapunkul and P. Iamprasertkun, Voltammetry Prediction and Electrochemical Analysis of Carbon Material from "Salt-In-Water" to "Water-In-Salt", *Anal. Chem.*, 2025, **97**, 3881–3891.
42 P. Simon and Y. Gogotsi, Materials for electrochemical capacitors, *Nat. Mater.*, 2008, **7**, 845–854.
43 J. Morán, J. Yon, C. Henry and M. R. Kholghy, Approximating the van der Waals interaction potentials between agglomerates of nanoparticles, *Adv. Powder Technol.*, 2023, **34**, 104269.
44 Q. P. Phan, T. C. L. Tran, T. T. Tran, T. T. H. La, X. V. Cao, T. A. Luu and T. Q. A. Luong, Synthesis of highly activated polybenzene-grafted carbon nanoparticles for supercapacitors assisted by solution plasma, *RSC Adv.*, 2024, **14**, 36610–36621.
45 A. J. Chancellor, B. T. Seymour and B. Zhao, Characterizing Polymer-Grafted Nanoparticles: From Basic Defining Parameters to Behavior in Solvents and Self-Assembled Structures, *Anal. Chem.*, 2019, **91**, 6391–6402.
46 Boonyeun, Rujiravanit and Saito, Deposition of carbon–tungsten carbide on coir pulp to improve its compatibility with polylactic acid, *Cellulose*, 2021, **28**, 4119–4136.
47 C. Singh and A. Paul, Physisorbed Hydroquinone on Activated Charcoal as a Supercapacitor: An Application of Proton-Coupled Electron Transfer, *J. Phys. Chem. C*, 2015, **119**, 11382–11390.
48 M. H. V. Huynh and T. J. Meyer, Proton-Coupled Electron Transfer, *Chem. Rev.*, 2007, **107**, 5004–5064.
49 C. Costentin, Electrochemical Approach to the Mechanistic Study of Proton-Coupled Electron Transfer, *Chem. Rev.*, 2008, **108**, 2145–2179.
50 D. K. Tran, S. M. West, E. M. K. Speck and S. A. Jenekhe, Observation of super-Nernstian proton-coupled electron transfer and elucidation of nature of charge carriers in a multiredox conjugated polymer, *Chem. Sci.*, 2024, **15**, 7623–7642.
51 A. Frontera, D. Quiñonero and P. M. Deyà, Cation–π and anion–π interactions, *Wiley Interdiscip. Rev.: Comput. Mol. Sci.*, 2011, **1**, 440–459.
52 C. Costentin, Electrochemical Approach to the Mechanistic Study of Proton-Coupled Electron Transfer, *Chem. Rev.*, 2008, **108**, 2145–2179.
53 J. Kröner, D. Platzer, B. Milow and M. Schwan, Electrical conductivity of monolithic and powdered carbon aerogels and their composites, *Mater. Adv.*, 2024, **5**, 8042–8052.
54 D. Pantea, H. Darmstadt, S. Kaliaguine and C. Roy, Electrical conductivity of conductive carbon blacks: influence of surface chemistry and topology, *Appl. Surf. Sci.*, 2003, **217**, 181–193.
55 M. S. Dresselhaus, A. Jorio, M. Hofmann, G. Dresselhaus and R. Saito, Perspectives on carbon nanotubes and graphene Raman spectroscopy, *Nano Lett.*, 2010, **10**, 751–758.